CONF-850708--1

TOKAMAK STARTUP—PROBLEMS AND SCENARIOS RELATED TO THE TRANSIENT PHASES OF IGNITED TOKAMAK OPERATIONS

John Sheffield

Oak Ridge National Laboratory
P.O. Box Y
Oak Ridge, Tennessee 37831

CONF-850708--1

DE85 015321

ABSTRACT

During recent years improvements have been made to tokamak startup procedures, which are important to the optimization of ignited tokamaks. The use of rf-assisted startup and noninductive current drive has led to substantial reduction and even complete elimination of the volt-seconds used during startup, relaxing constraints on poloidal coil, vacuum vessel, and structure design. This paper reviews these and other improvements and discusses the various bulk heating techniques that may be used to ignite a D-T plasma.

I. STARTUP TECHNIQUES AND STUDIES

I.1 Introduction

Extensive studies have been made of the startup to ignition of tokamaks, notably for INTOR[1] and FED/TFCX.[2,3] Even during the relatively short timescale of these studies there have been substantial advances in startup techniques, which have led to overall improvements in the ignited tokamak design and cost. The key improvements are:

- minimization of the voltage per turn needed to set up the plasma current, which permits the use of a lower-voltage poloidal coil system and a lower resistance vacuum vessel;
- minimization of the volt-seconds used in raising the plasma current, which simplifies the poloidal coil system; and
- minimization of the bulk heating auxiliary power requirements, which relates to finding the optimum route for raising I_p, T, and n from the plasma initiation levels to the plasma burn levels.

The advances are well illustrated by a plot of the loop voltage behavior during the initial phase of the discharge. From 1982 to 1984, estimates of the requirements have decreased from 100 V per turn to 10 V per turn for an optimized startup, as illustrated in Fig. 1. New results, discussed below, show that with lower hybrid preionization and current drive the voltage may even be reversed.

Research sponsored by the Office of Fusion Energy, U.S. Department of Energy, under contract DE-AC05-84OR21400 with Martin Marietta Energy Systems, Incorporated.

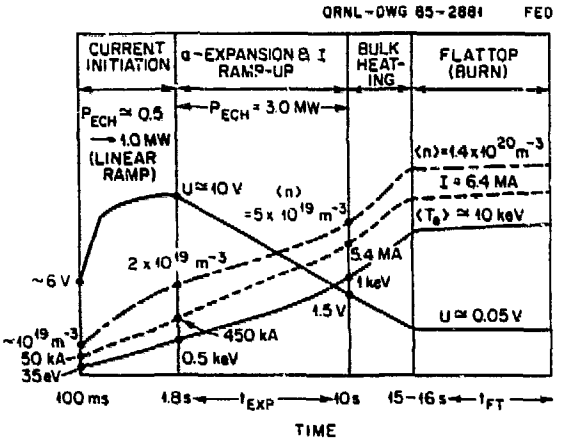

Fig. 1. Diagram of startup to ignition in an INTOR-scale tokamak using rf-assisted startup (courtesy of S. Borowski, ORNL-FEDC, TM-83-8).

The main elements of this phase of operation are:

- the poloidal coil system and plasma position control;
- the vacuum vessel and structure (eddy currents, disruptions);
- preionization and preheating;
- type of current rampup, inductive or noninductive;
- density control, gas puffing, pellets, pumped limiter/divertor; and
- impurity control—impurity minimization, flow reversal, divertors.

The key physics elements that constrain operation are:

- ion, electron and impurity transport;
- MHD effects—disruptions, q_ψ limit, magnetic reconnection; and
- beta limit[4] and Murakami density limit.[5]

The limits on the plasma parameters' operating space are illustrated in Fig. 2 with a POPCON plot.[6] Three cases are shown:

- in Fig. 2a, moderate auxiliary power by neutral beam heating leads to ignition—the optimum route; the "Cordey pass"[7] minimizes the power requirements;
- in Fig. 2b the plasma ignites by ohmic heating alone, through the use of very high field and low q_ψ (ref. 8); and
- in Fig. 2c the beta and Murakami limits occur before ignition is achieved—note that even in this case there may be high energy gain Q (ref. 2).

The two papers presented at this workshop concentrate on the use of ignition tokamaks that require auxiliary heating to ignite, though brief comments will be made on ohmic ignition. A large part of the discussion will be on optimizing startup, which is a common issue for both cases. The first section of this paper covers the plasma initiation and current rise phase. The second section covers bulk heating to ignition. A detailed discussion of impurity minimization and control is beyond the scope of this paper.

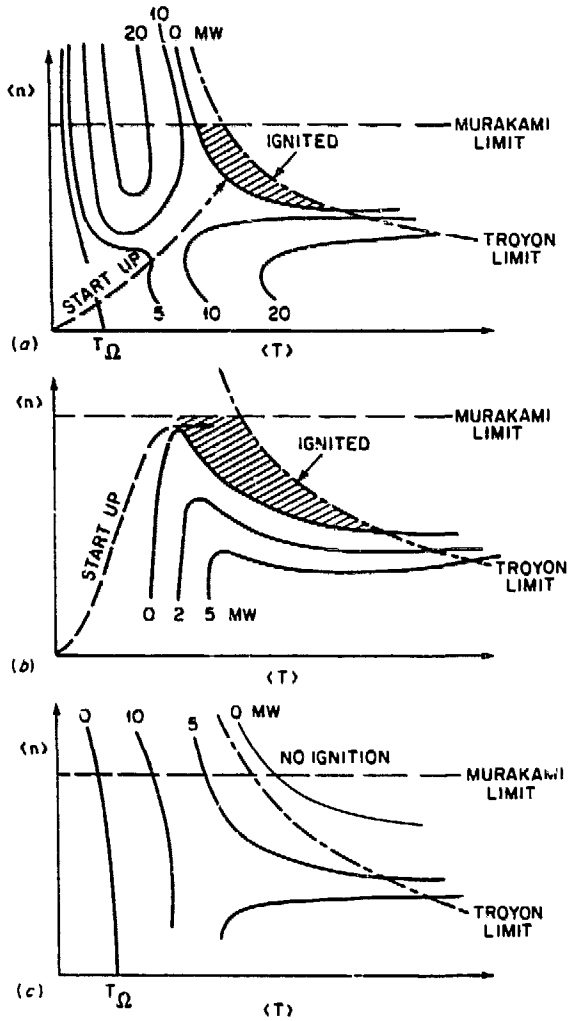

Fig. 2. Plasma OPeration CONtour (POPCON) plots. (a) Neutral beam heating to ignition, (b) ohmic heating to ignition, (c) a high-Q nonignited case.

I.2 Particle and Plasma Power Balance

The state of the plasma in a tokamak is determined by the detailed balance of particle production and loss and of power input and loss. In a plasma quasi-neutrality holds; that is, $(n_e - n_i)/n_e << 1$, so $n_i \simeq n_e$. However, although the base plasma may be predominantly deuterium and tritium, there are always more massive impurities n_Z. When ionized, these become multiply charged ($Z > 1$) so that in general $n_i < n_e = n_i + \sum_Z Z n_Z$, where Z is the charge state of each impurity ion. A convenient measure of the impurity level is the parameter

$$Z_{\text{eff}} = \frac{\sum_Z Z^2 n_Z + n_i}{n_e} \,. \tag{I.1}$$

The particle balance in a basically single-ion-species plasma, setting $n_e = n_i$, is given by

$$\frac{\partial n}{\partial t} = n n_n \langle \sigma v \rangle_i + \frac{1}{r} \frac{\partial}{\partial r} \left(r D_A \frac{\partial n}{\partial r} \right) \left(\mathrm{m}^{-3} \cdot \mathrm{s}^{-1} \right) , \tag{I.2}$$

where $\langle \sigma v \rangle_i$ is the ionization rate[9] of the neutral particles that fuel the plasma. The plasma system will maintain charge neutrality, and the electron and ion diffusion rates D_e and D_i are equal to each other and to the ambipolar diffusion rate D_A. The power balance may be written separately for each species. For the electrons, the local power balance is given by

$$\frac{\partial}{\partial t} \left(\frac{3}{2} n_e e T_e \right) = \frac{1}{r} \frac{\partial}{\partial r} r \left(n_e e \chi_e \frac{\partial T_e}{\partial r} + \frac{3}{2} T_e e D_A \frac{\partial n_e}{\partial r} \right)$$

$$+ p_{ie} - p_b - p_R - p_c + p_\Omega + p_{\alpha e} + p_{ae} \left(\mathrm{W} \cdot \mathrm{m}^{-3} \right) . \tag{I.3}$$

For the ions, the local power balance is given by

$$\frac{\partial}{\partial t} \left(\frac{3}{2} n_i e T_i \right) = \frac{1}{r} \frac{\partial}{\partial r} r \left(n_i e \chi_i \frac{\partial T_i}{\partial r} + \frac{3}{2} T_i e D_A \frac{\partial n_i}{\partial r} \right)$$

$$+ p_{ei} - p_{cx} + p_{\alpha i} + p_{ai} \left(\mathrm{W} \cdot \mathrm{m}^{-3} \right) . \tag{I.4}$$

In addition, there are similar equations for each impurity ion species where, generally, collisions between ion species maintain $T_Z \sim T_i$. The transport of impurities is complex, depending on details of the plasma parameter gradients, and impurities may move either radially in or out with respect to the background plasma. This is a basis for impurity control.[10,11,12]

The parameters χ_e and χ_i are the electron and ion thermal diffusivities, respectively, and p $(\mathrm{W} \cdot \mathrm{m}^{-3})$ is the power density of the various mechanisms indicated by the subscripts:

ei	electron-ion collisions	Ω	ohmic heating
b	bremsstrahlung	α	alpha power
R	radiation	a	auxiliary power
c	cyclotron radiation	cx	charge exchange.

These contributions are discussed below. To simplify the equations we get $n_i = n_e = n$.

I.2.1 Electron-ion heat transfer

The electron-ion heat transfer[13] is

$$p_{ei} = -p_{ie} = 3\nu_{ei} n \frac{m_e}{m_i} e(T_e - T_i) \tag{I.5}$$

where

$$\nu_{ei} = 2.92 \times 10^{-12} n T_e^{-3/2} \ln \Lambda \ (s^{-1}) \tag{I.6}$$

and

$$\Lambda = (1.53 \times 10^{12}) n^{-1/2} T_e^{3/2} \tag{I.7}$$

represents the collisional transfer of power between electrons and ions.

I.2.2 Bremsstrahlung radiation

Bremsstrahlung radiation[14] is

$$p_b = 1.7 \times 10^{-38} \quad \xi n_e^2 Z_{eff} T_e^{1/2} \tag{I.8}$$

where the Gaunt factor ξ corrects for electron-electron collisions; and relativistic effects, for 1 keV $< T <$ 50 keV, $1 < \xi < 1.2$.

I.2.3 Impurity Line Radiation

Radiation[15] is

$$p_R \approx n \sum_Z n_Z f(Z) \ , \tag{I.9}$$

where, as shown in Fig. 3, $f(Z)$ for the example case of oxygen varies strongly with changing T_e.

I.2.4 Cyclotron radiation

There is no universal formula for cyclotron radiation[16] because of the differing behavior with changing temperature of the various harmonics. For the temperatures encountered up to ignition, typically $T_e \lesssim 25$ keV, an adequate approximation is

$$p_c = \frac{4.8 \times 10^{-16} n_e^{0.5} T_e^{2.1} B^{2.5} (1 - R_e)^{0.5}}{\bar{a}} \ , \tag{I.10}$$

where $R_e = 0.95$ is the wall reflectivity.

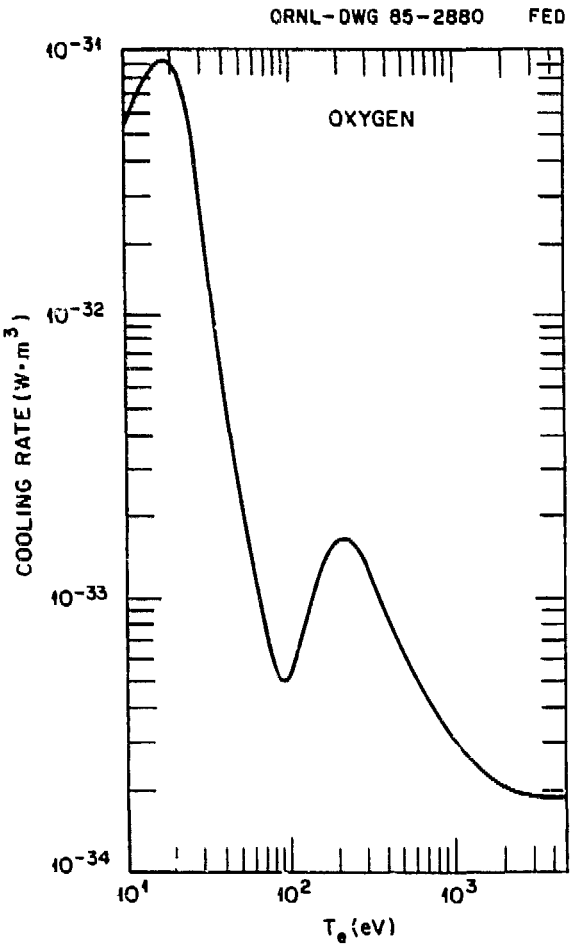

Fig. 3 The radiation cooling rate of $f(Z)$ is shown as a function of T_e for oxygen radiation (courtesy of E. C. Crume, ORNL).

I.2.5 Ohmic heating

Ohmic heating is

$$p_\Omega = \eta_\parallel j^2 = \frac{7.53 \times 10^{-5} \gamma_R Z_{\text{eff}} j^2 \ln \Lambda}{T_e^{3/2}} , \tag{I.11}$$

where γ_R is a neoclassical resistivity correction factor allowing for trapped electron effects; and j (A·m^{-2}) is the local plasma current density, $j = E/\eta_\parallel$; the parallel resistivity is $\eta_\parallel = 7.53 \times 10^{-5} Z_{\text{eff}} \ln \Lambda / T_e^{3/2}$; and $\gamma_R \simeq (1 - 1.95\,\epsilon^{1/2} + 0.95\epsilon)^{-1}$, $\epsilon = r/R$.

I.2.6 Alpha power

For the D-T cycle,

$$\begin{gathered} {}^2_1\mathrm{D} + {}^3_1\mathrm{T} \rightarrow {}^4_2\mathrm{He} + {}^1_0\mathrm{n} \\ 3.52 + 14.06 = 17.58\ \text{MeV} = E_n \ . \end{gathered} \tag{I.12}$$

The fusion power density is

$$p_F = n_D n_T \langle \sigma v \rangle_F E_n \ . \tag{I.13}$$

Convenient empirical formulae for the alpha power density are, for 2 keV $\leqslant T_i \leqslant$ 35 keV,

$$p_\alpha \simeq 2 \times 10^{-34} \frac{n_D n_T}{T_i^{2/3}} \exp\left[\frac{-200}{T_i^{1/3}}\right] ; \tag{I.14}$$

and, for 2 keV $\lesssim T_i \lesssim$ 10 keV,

$$p_\alpha \simeq 4.0 \times 10^{-57} n_D n_T T_i^4 \ . \tag{I.15}$$

Note that for $T_e \lesssim 25$ keV the bulk of the alpha power ($\gtrsim$70%) is transferred to the electrons [see Eq. (II.15)].[17] Nevertheless, if $\chi_i <<< \chi_e$ it is possible to have $T_i > T_e$.

I.2.7 Auxiliary power

The distribution of auxiliary power in radius and between electrons and ion depends upon the type of heating, as discussed in Sect. II.5.

I.2.8 Charge exchange

The charge exchange is

$$p_{cx} = n n_n \langle \sigma v \rangle_{cx} \frac{3}{2} e(T_i - T_n) \ , \tag{I.16}$$

where $\langle \sigma v \rangle_{cx}$ is the rate coefficient.[9] This term is important during discharge initiation and under all circumstances at the plasma edge where neutral recycling occurs.

I.3 Particle and Plasma Power Balance

The total power flow pattern in a tokamak is illustrated in Fig. 4. Emphasis is placed there on two regions, the interior and the edge, which generally differ markedly in character. In the interior out to about one-half or two-thirds of the radius, the power input, both ohmic and auxiliary, is lost primarily by conduction and diffusion (convection). Under typical good conditions in present tokamaks, radiation and charge exchange losses in the interior are small. In the outer regions of the plasma, partially ionized low-Z impurities emit large amounts of radiation. In addition, hydrogen neutrals recycling from the wall charge-exchange on plasma ions, leading to further losses. The ideal tokamak magnetic topology consists of nested magnetic surfaces. Transport across those surfaces is then by diffusion and conduction owing to Coulomb collisions as the charges follow classical orbits. In reality, a saturated level of plasma fluctuations can occur. These fluctuations may distort the magnetic field connecting field lines radially or set up electric fields that enhance transport. The picture of the power flow may be subdivided further to

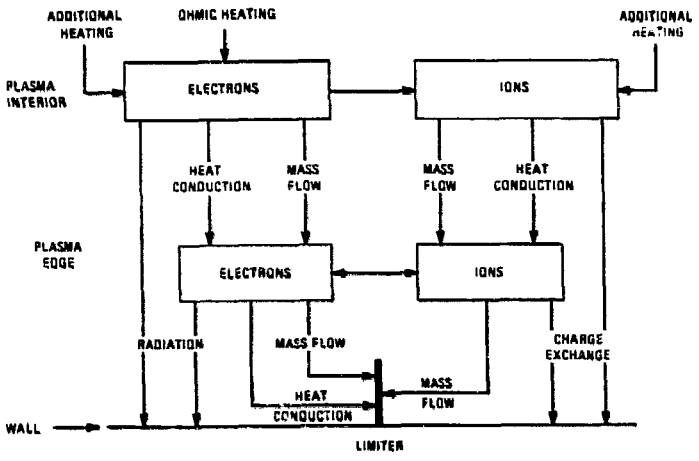

Fig. 4. Energy flow pattern in the tokamak.

bring out the effect of these macroscopic fluctuations in the plasma. In the center of the plasma, it is common for the safety factor q_0 to drop below unity as the center heats. When this occurs, an unstable $m = 1$ mode drives the temperature down until $q_0 > 1$. A relaxation oscillation ensues with a characteristic sawtooth behavior. This mode leads to convection of heat that can dominate the power balance in the center. Farther out in radius where the gradients are strong, microscopic modes are observed and are believed to account for the anomalously high electron transport. The various regions are illustrated with a radial power balance in TFR, Fig. 5.

I.4 Startup

In the INTOR[1] studies, four phases of startup are identified:

1. ionization and current initiation phase,
2. phase of current rise at low electron temperature, $T_e \leq 100$ eV,
3. phase of current rise at medium electron temperature, 100 eV $\lesssim T_e \lesssim$ 1 keV, in which the current reaches its maximum value and the main ohmic heating takes place, and
4. bulk heating of the plasma to ignition.

A typical scenario is illustrated in Fig. 1, where the variation of loop voltage U, average density $\langle n \rangle$, average electron temperature $\langle T_e \rangle$, and plasma current I_p are shown. Phase 3 varies depending on whether (a) inductive current drive is used (as shown), or (b) noninductive current drive and lower density are used.

I.4.1 Ionization and current initiation

A key issue is the loop voltage required for startup, as this has a strong impact on the poloidal coil and vacuum vessel design. Typically, at an initial hydrogen pressure, $p = (0.6\text{–}3) \times 10^{-4}$ torr, the breakdown electric field strength $E =$ 1–2.5 V/m (ref.1). The loop voltage $U = 2\pi RE$; so, for example, an ignition tokamak with $R = 4$ m has $U \sim$ 26–60 V. The breakdown voltage and subsequent voltage behavior depend on the electron loss channels, which include toroidal drift, transverse diffusion, recombination and attachment (e.g., to oxygen atoms), and

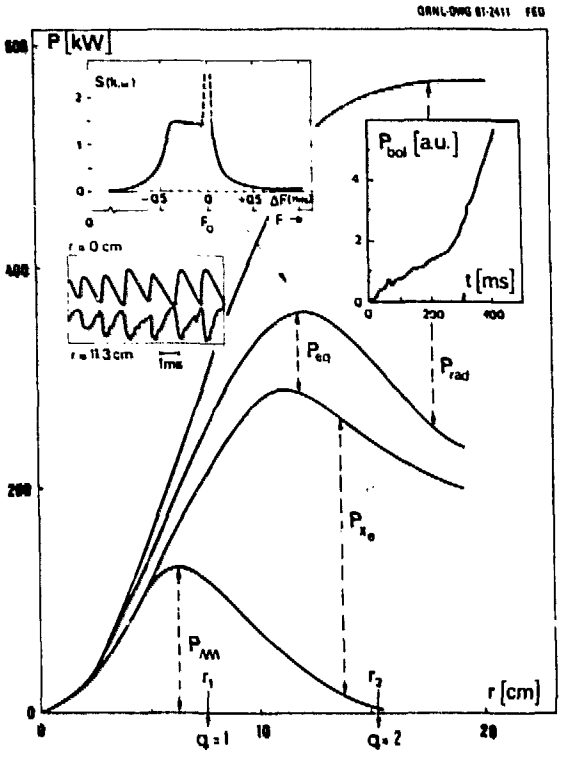

Fig. 5. Power balance for a TFR plasma. In the inserts are shown the experimental results for the dominant physical mechanism in each of the the three plasma regions: sawtooth activity, microturbulence, and spectral radiation (courtesy of J. Tachon, CEN, Fontenay-aux-Roses).

poloidal stray magnetic fields ($B_\perp$). If the latter factor dominates ($B_\perp > 10^{-4} B_t$) the requirement on electric field[18] is

$$E \geqslant E_{\min} = 1.3 \times 10^4 p/\ln(530 paB_t/B_\perp)\ (\mathrm{V \cdot m^{-1}}) \tag{I.17}$$

where p(torr), a(m).

Preionization by electron cyclotron heating (ECH)[19] has proved effective in reducing the breakdown voltage in tokamaks.[20–22] It also makes the startup less sensitive to the initial impurity levels. At very low electron density, the microwave power in the extraordinary mode is absorbed at the cyclotron resonance by single-profile resonance effects, generating electrons with an energy high enough to induce significant ionization. The density rises locally, and the absorption moves to the region of the upper hybrid resonance.[21] Ignoring the question of plasma instability at low (zero) plasma current, one may obtain an estimate of the initial plasma parameters from an analysis of the particle and energy balances. In regions where $B_\perp$ is low, curvature-induced drift dominates the electron losses, and Eq. (I.2) becomes

$$n_e n_n \langle \sigma v \rangle_i = \frac{n_e}{\tau_{D_e}}\ (\mathrm{m^{-3} \cdot s^{-1}}) \tag{I.18}$$

where

$$\tau_{D_n} = \tau_{D_i} = 0.5\, bR\frac{B_t}{T_e}\ (\mathrm{s})\ .$$

The electron energy balance, Eq. (I.3), in quasi steady state becomes

$$p_\mu + p_\Omega = \epsilon_i\, n_e n_n \langle\sigma v\rangle_i + p_{ei} + \frac{3}{2} n_e \frac{T_e}{\tau_{D_e}} + p_R\ . \tag{I.19}$$

The effective ionization energy for hydrogen is $\epsilon_i \simeq 40$ eV, including excitation losses; p_μ is the microwave power density.

For the ions the power balance, Eq. (I.4), reduces to

$$p_{ei} + \frac{3}{2} n_e n_n T_n \langle\sigma v\rangle_i = \frac{3}{2} n_e\left[(T_i - T_n) n_n \langle\sigma v\rangle_{cx} + \frac{T_i}{\tau_{D_i}}\right]\ . \tag{I.20}$$

The second term on the left side of Eq. (I.20) represents the energy going to the ions from the ionization of neutrals.

Combining Eqs. (I.18)–(I.20) leads to

$$p_\mu + p_\Omega = \left[\frac{2}{3}\epsilon_i + T_e + (T_i - T_n)\frac{\langle\sigma v\rangle_{cx}}{\langle\sigma v\rangle_i} - T_n + T_i\right]\frac{3 n_e e T_e}{brB_t} + p_R\ . \tag{I.21}$$

For ISX-B these equations produce parameters consistent with the observed plasma parameters; namely, for $B_t = 1.3$ T, $R = 0.96$ m, $b = 0.27$ m, and 80 kW of ECH power at 35 GHz, the average density $\bar{n}_e = 3 \times 10^{18}\ \mathrm{m}^{-3}$, $\overline{T_e} = 10$ eV and $T_e(\mathrm{peak}) \simeq 50$ eV near the upper hybrid resonance layer.

In ISX-B spectroscopic and radiometric data showed that radiation was not the dominant loss mechanism; nevertheless, small amounts of, for example, oxygen (density n_0) can lead to substantial losses. For an INTOR-scale tokamak the appropriate parameters are $a = 1.2$ m, $b = 1.9$ m, $R = 5$ m, $B_t = 5$ m, $\epsilon_i = 40$ eV; for $\bar{n}_e = 3 \times 10^{18}\ \mathrm{m}^{-3}$, $T_e = 20$ eV, $T_i = 10$ eV, $T_n = 3$ eV, $\langle\sigma v\rangle_{cx}/\langle\sigma v\rangle_i \simeq 3$, and $f(Z) \simeq 8 \times 10^{-32}\ \mathrm{W\cdot m^{-3}}$ for oxygen, as shown in Fig. 3.

The required microwave power density for preionization ($p_\Omega = 0$) is

$$p_\mu \simeq \left[50 + 7.2 \times 10^5 \frac{n_0}{n_e}\right]\ (\mathrm{W\cdot m^{-3}})\ , \tag{I.22}$$

and clearly oxygen radiation will dominate the losses if $n_0/n_e > 10^{-4}$ and stray fields are small ($B_\perp < 2$ G for INTOR). The total microwave power to produce

plasma in the ultimate plasma volume is

$$P_{\mu} \simeq 1.7 \times 10^{2} \frac{n_0}{n_e} \quad \text{(MW)} \ . \tag{I.23}$$

Thus oxygen levels should be kept to $n_0/n_e \leq 0.02$, and then a few megawatts of ECH should be adequate for preionization.

The use of preionization removes the initial peak in the loop voltage, required otherwise for breakdown, as shown in the data from ISX-B[21] in Fig. 6. At the same time, it permits a greater rate of current rise. The volt-seconds used during this preionization and initial current ramp phase were reduced by 30% owing to a substantial reduction in the resistance component.

Computations of the startup phase of INTOR are shown in Fig. 1. The use of a few megawatts of ECH is computed to overcome the oxygen radiation barrier and to raise the electron temperature to ~100 eV and the density to a level approaching 10^{13} m^{-3} during the first few milliseconds of the discharge. For the INTOR case, the stray poloidal field may be dominant, and the power required increases to 8 MW. The use of ECH power may reduce the peak loop voltage to as low as 10 V, as shown in Fig. 1.

Recently in PLT[23] lower hybrid power has been used for preionization and current ramp to the 100-kA level, as shown in Fig. 7. Similar results have also been obtained in Asdex, and in both cases the loop voltage is actually reversed, leading to recharging of the transformer. Current rampup is discussed in more detail in Sect. 1.4.4.

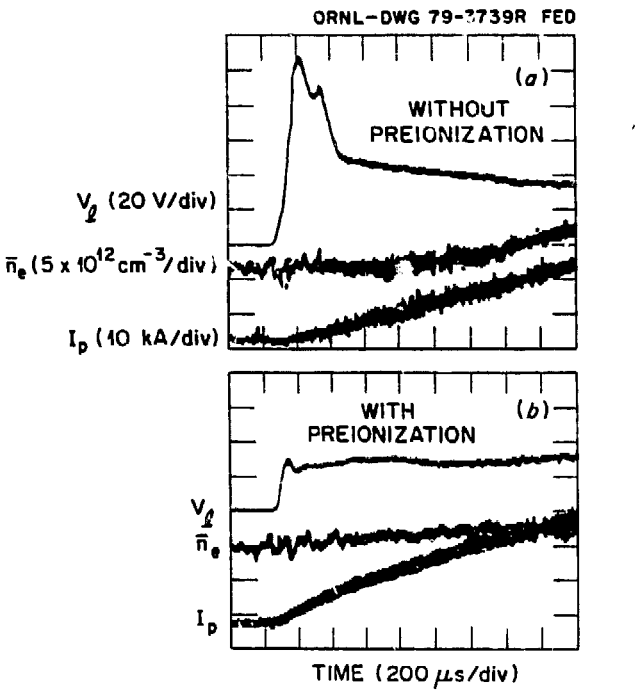

Fig. 6. The reduction of volt-seconds used in startup by the application of ECH in ISX-B: (a) without preionization, $U > L(dI_p/dt)$; (b) with preionization, $U \simeq L(dI_p/dt)$ (courtesy of A. England, ORNL).

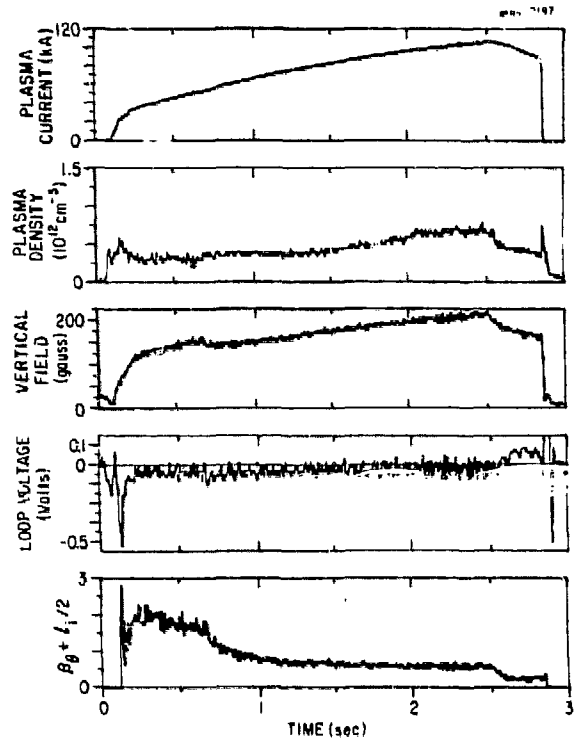

Fig. 7. Lower hybrid power of 180 kW is used to preionize and ramp the plasma current in PLT (courtesy of S. Bernabei, PPPL).

I.4.2 Torus and poloidal coil system

The use of ECH-assisted startup removes the need to use a high resistive torus structure and high-voltage superconducting poloidal coils. A high resistance torus is desirable from the point of view of magnetic field penetration, to reduce eddy current losses during startup. On the other hand, a low resistance torus acts to stabilize external kink modes[25] and can minimize disruption damage. In a major disruption there is a fast transient phase (thermal quench) in which the plasma transfers a major part of its thermal energy to the limiters and walls. The current quench phase is longer than the thermal phase, and with an inadequately conducting torus a large percentage of the greater self-inductance energy is transferred to the plasma and then to the wall. A low-resistance toroidal path slows the current density decay in a disruption and reduces the interaction with the coils. This effect, together with the the lower-voltage startup, also permits the use of a lower voltage superconducting transformer primary and vertical field coils, or alternatively releases volt-seconds for use during the burn phase.

I.4.3 Volt-second usage

The loop voltage has both an inductive and a resistive component.

$$U = \frac{d}{dt}(LI_p) + R_p I_p \quad \text{(V)} \ , \tag{I.24}$$

where R_p is the plasma resistance. The parallel resistivity in the magnetic field is given by

$$\eta_{\parallel} = \frac{7.53 \times 10^{-5} \gamma_R Z_{eff} \ln \Lambda}{T_e^{3/2}} \ (\Omega \cdot m) \tag{I.25}$$

where γ_R corrects for trapped electron effects. Profile effects are important, and tailoring the current profile may be used to minimize volt-seconds usage.

Ignoring variations in γ_R, Z_{eff}, and ln Λ and taking a parabolic electron temperature profile leads to a plasma resistance for a noncircular plasma of

$$R_p \simeq \frac{3.8 \times 10^{-4} R \gamma_R Z_{eff} \ln \Lambda}{ab T_{e0}^{3/2}} \ (\Omega) \ , \tag{I.26}$$

where T_{e0} is the central electron temperature.

The plasma–poloidal coil inductance may be approximated by a coaxial toroidal inductance, and

$$L = \mu_0 R \left[\ln \left(\frac{a_{pol}}{a} \right) + 0.25 \right] \ (H) \ , \tag{I.27}$$

where a_{pol}/a is the ratio of the poloidal coil radius to the plasma minor radius.

As an example, consider the current rise phase to $I_p = 5$ MA at $T_{e0} = 2$ keV on an INTOR-scale device with $R = 5$ m, $a = 1.2$ m, $b = 1.9$ m, $a_{pol}/a \simeq 2$, $\mu_0 = 4\pi \times 10^{-7}$ (H/m), $\gamma_R Z_{eff} = 1.5$, and ln $\Lambda = 18$. The volt-seconds usage from $t = 0 \rightarrow t = \tau$ is given by

$$\text{V·s} = LI + \int_0^{\tau} R_p I_p \, dt \ . \tag{I.28}$$

If one assumes a linear rise of I_p and T_{e0}, then the total volt-seconds used in a time $\tau = 10$ s is

$$\text{V·s} \simeq 30 \text{ (inductive)} + 18 \text{ (resistive)} \ .$$

If assisted startup is used so that the current is raised mainly when $T_{e0} \geq 200$ eV, then the effective startup time becomes $t = 1.0 \rightarrow 10$ s and

$$\text{V·s} \simeq 30 + 12 \text{ (resistive)} \ .$$

These results are consistent with the common experience[26] that the total volt-seconds for inductive startup without assistance is V·s $\simeq (1.5\text{–}2.0) LI_p$. The use of assisted startup techniques to cut initial resistive losses and careful programming of the plasma current and density to avoid MHD effects (which enhance energy losses and lower T_{e0}) make it possible to obtain V·s $< 1.5\, LI_p$.

I.4.4 Current rampup

Inductive rampup. It is commonly observed that current penetration radially in a tokamak is faster than would be expected from classical resistive diffusion.[27–29] The observation of MHD oscillations indicates that the enhanced penetration is due to magnetic reconnection caused by tearing modes. In particular, with a fast rate of current rise in small devices ($\dot{I}_p \simeq 10$ MA/s), a hollow electron temperature profile is observed, and theoretically this should lead to the double tearing mode instability.[30] For a flat central q-profile the plasma may still be unstable to a single-helicity mode.[30] The MHD activity and the rate of current penetration increase with the increasing current rise.[31]

A computer prediction of current rampup in ISX-B is shown in Fig. 8 (ref. 32) using diffusion and a penetration model based on tearing modes.[31] From a practical point of view, the dominant rate of rise is a trade-off between minimizing the volt-seconds used during the current rise and simultaneously minimizing MHD-generated transport increases (which by reducing the electron temperature increase the volt-seconds used). A limit is also set by the increasing disruptivity observed as $\dot{I}_p$ is increased. In the new generation of large tokamaks, such as TFTR and JET,[33,34] rates of current rise $\dot{I}_p \simeq 1$ MA/s are found to be optimum.

Noninductive rampup. Numerous techniques[35] have been proposed for noninductive current drive. These include:

- neutral beam injection, which has been observed to lower the loop voltage and drive plasma current in DITE,[36]
- relativistic electron beam injection, which has been studied in Macrotor,[37] and
- rf wave current drive, which is the most successful technique and is discussed below.

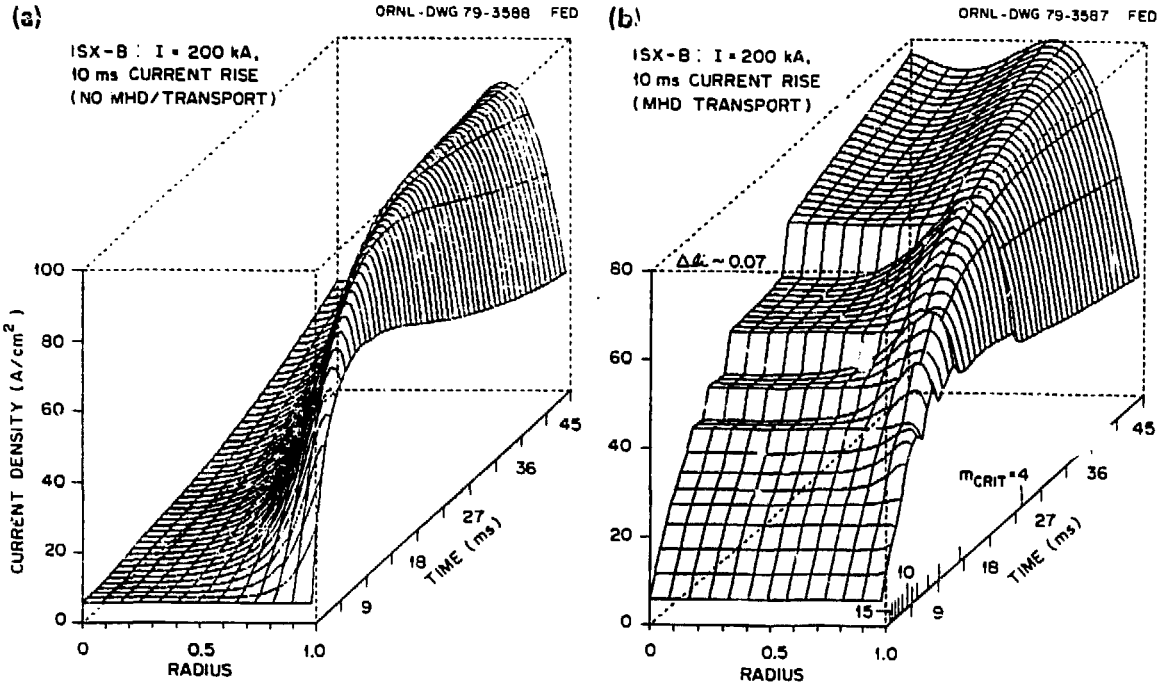

Fig. 8. Computer simulations of ISX-B. (a) Classical resistivity leads to a skin current, while (b) double tearing mode activity enhances current penetration (courtesy of W. Houlberg, ORNL).

An important figure of merit is the current driven per unit power input. This is illustrated in Fig. 9 for a variety of techniques. It is possible to inject rf power (P_{rf}) into a plasma in a way that transfers axial momentum to one of the charge species. One such scheme relies upon the Landau damping of high-phase velocity (V_{ph}) waves launched in one direction parallel to the magnetic field.[38] In fact, any technique that leads to a net drift asymmetry in the parallel velocity distribution function of one set of charges can contribute a current, provided a compensatory effect does not occur in the other charge species.

There are three main categories of rf current drive:

- high-speed waves with phase velocities that are several times the electron thermal speed,
- low-speed waves with subthermal phase speeds, which have the most momentum per unit energy—for example, the fast wave (i.e., compressional Alfvén wave at low frequencies and the magnetosonic wave above the ion cyclotron frequency), and
- selective heating which creates an anisotropic particle distribution and indirectly drives current. Examples are ion cyclotron heating (ICH) and ECH.

The current density is defined as

$$\vec{J} = n_e \vec{V}_{rel} \ , \tag{I.29}$$

where V_{rel} is the relative velocity of the ion and electron species.

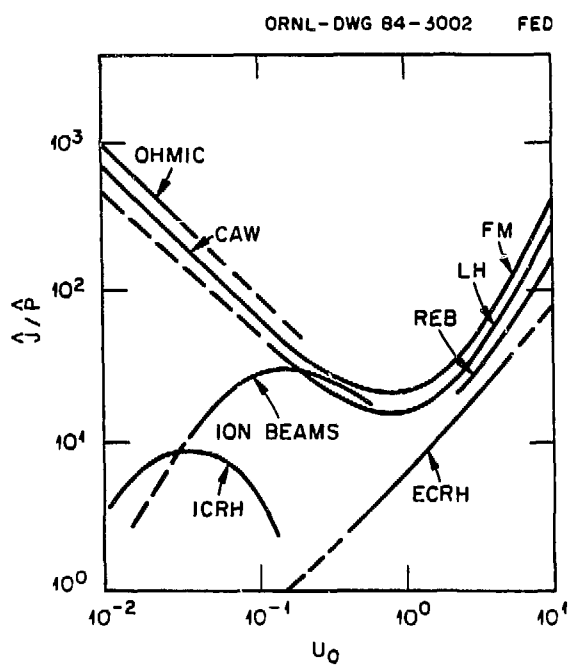

Fig. 9. Normalized efficiency factor vs $U_0 = (\omega - l\omega_c)/k_\parallel v_e$, with ω_c the cyclotron frequency for waves and $U_0 = V_b/v_e$ for particle injection at V_b (courtesy of N. Uckan, ORNL).

The Coulomb collisional force on the current carriers is

$$\vec{F} = mn\nu\,\vec{V}_{rel} \ ,$$

where m is the mass of the carrier particle and ν is the collision frequency.

The power to maintain the current is

$$P = \vec{F} \cdot \vec{V}_{rel} = mn\nu\, V_{rel}^2 \ (\mathrm{W \cdot m^{-3}}) \ . \tag{I.30}$$

It is conventional to introduce normalized values

$$\hat{J} = \frac{J}{ne v_e} \ , \quad \hat{P} = \frac{P}{m_e n v_e^2 \nu_0} \ , \tag{I.31}$$

where $J = |\vec{J}|$, $v_e = (kT_e/m_e)^{1/2}$ is the electron thermal speed, and $\nu_0 = \omega_{pe}^4 \ln \Lambda / 2\pi n v_e^3 = ne^4 \ln \Lambda / 2\pi\epsilon_0^2 m_e^2 v_e^3$.

Combining these equations leads to

$$\frac{\hat{J}}{\hat{P}} = \frac{m_e \nu_0}{m\nu} \frac{1}{U_0} \ , \tag{I.32}$$

where $U_0 = V_{rel}/v_e$, and ν_0/ν is a function of U_0. Figure 10 shows the variation of these quantities obtained when a detailedcalculation is made of ν_0/ν for a particular current drive scheme.[39]

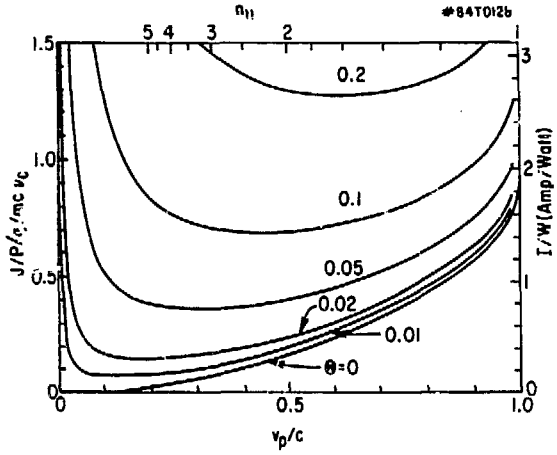

Fig. 10. Efficiencies for narrow Landau spectrum as a function of the phase velocity V_{ph}; in all cases $Z = 1$. The top scale gives the parallel index of refraction $n_\parallel = c/V_{ph}$. The right scale gives efficiency for $n = 10^{20}\,\mathrm{m}^{-3}$, $\ln \Lambda = 15$, and $R = 1$ m (courtesy of N. Fisch, PPPL).

In the ideal situation the current per unit of power for rf-driven electrons may be written as

$$\frac{I_{rf}}{P_{rf}} = \frac{e}{2\pi R m_e \nu_{ei} v_e} \times \begin{cases} A_1 \left(\dfrac{V_{ph}}{v_e}\right), & V_{ph} < v_e \\ A_2 \left(\dfrac{V_{ph}}{v_e}\right), & V_{ph} > v_e \end{cases} \tag{I.33}$$

where V_{ph} is the phase velocity of the wave and ν_{ei} is the electron-ion collision frequency. Detailed calculations give values for the constants of $A_1 \simeq 0.023$ and $A_2 \simeq 1.0$. The most commonly used technique is lower hybrid current drive (LHCD). The lower hybrid frequency is $\omega_{LH} = [\omega_{pi}^2/(1 + \omega_{pe}^2/\Omega_e^2)]^{1/2}$ where ω_{pi} and ω_{pe} are, respectively,, the ion and electron plasma frequencies and Ω_e is the electron cyclotron frequency.

In PLT[40] at densities in the range (4–6) $\times$ 10^{18} m^{-3} with a 90° phase difference between waveguides on a six-waveguide array, the observed efficiency was

$$\frac{I_{rf}}{P_{rf}} \simeq \frac{0.8}{\langle n_{19} \rangle (R/1.3)} \quad (A \cdot W^{-1}) .$$

There are three important features of the "efficiency": it is inversely proportional to the major radius R and to the density $\langle n \rangle$, and there is a maximum density for LHCH set by the accessibility condition to the resonance zone. Relativistic effects modify the formula [Eq. (I.33)], and for the temperatures of D–T burning fusion plasmas, they act to improve the efficiency as shown in Fig. 10 (ref. 41).

The density dependence is well illustrated by the plot in Fig. 11 from Alcator C (ref. 42) of efficiency vs density. A summary of results of LHCD in a variety of experiments is given in Fig. 12.

Tokamak discharges have been initiated and the current density ramped up from zero by LHCD alone.[23,43] This development, coupled with ECH-assisted startup, has the potential nearly to eliminate (and, with recharging of the transformer, to eliminate) net inductive volt-seconds used during the entire startup phase.

The rate of current rise is ignited by the tendency of electrons to run away in the counterdirection. In lower hybrid current rampup, as the rf-driven current rises, a toroidal dc electric field is induced, which acts to produce a countercurrent. If the counter E-field is very strong, then electrons may runaway in the counterdirection.[44] In addition, the modification of the electron distribution function by the rf heating and by the E-field act to increase the conductivity, and this in turn increases the L/R_p time of the plasma and limits the rate of current rise.[45] The results of rampup tests in PLT are shown in Fig. 13, where the efficiency[46] of rampup is defined as

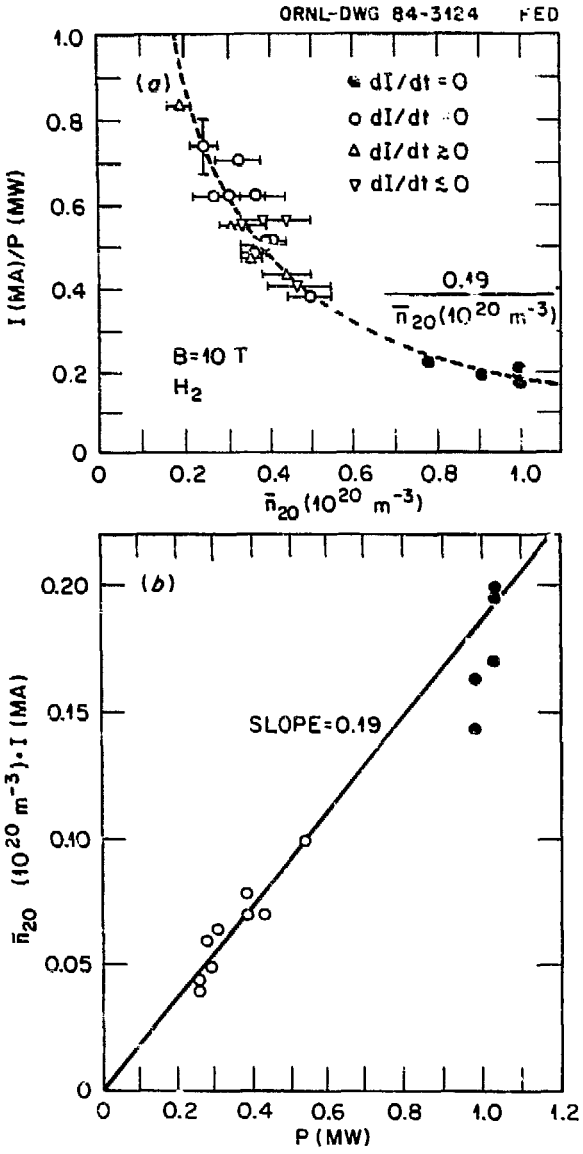

Fig. 11. Lower hybrid current drive efficiency in Alcator-C decreases as expected with increasing density (courtesy of M. Porkolab, MIT).

$$\epsilon = \frac{\dot{W}'}{P_{rf}} \lesssim 0.25 \ .$$

$\dot{W}' = \dot{W} - P_{ext}$, where $\dot{W}$ is the rate of change of inductive energy and P_{ext} is the component coming from the poloidal field system. For a lower hybrid power of 260 kW delivered from a six-waveguide array to a plasma with a density of 2.2×10^{18} m^{-3} and a temperature of about 1 keV, the rate of current rise was $\dot{I}_p \simeq 120$ kA/s ($\dot{W} \simeq 82$ kW, $P_{ext} \simeq 19$ kW) and $\epsilon \simeq 0.24$. Directional measurements of X rays showed an increase in the backward emission, supporting the thesis that the electron field in the plasma is reversed. The results are consistent with the theoretical model[44] (see Fig. 14). The model has been used to estimate the power requirements for an ignition tokamak ($R \simeq 3$ m, $L \simeq 8$ μH): to ramp up to 10 MA in 30 s, at $n = 5 \times 10^{18}$ m^{-3} and $T = 1$ keV, would take $E \simeq 0.6$ V/m and an average rf power of 40 MW.

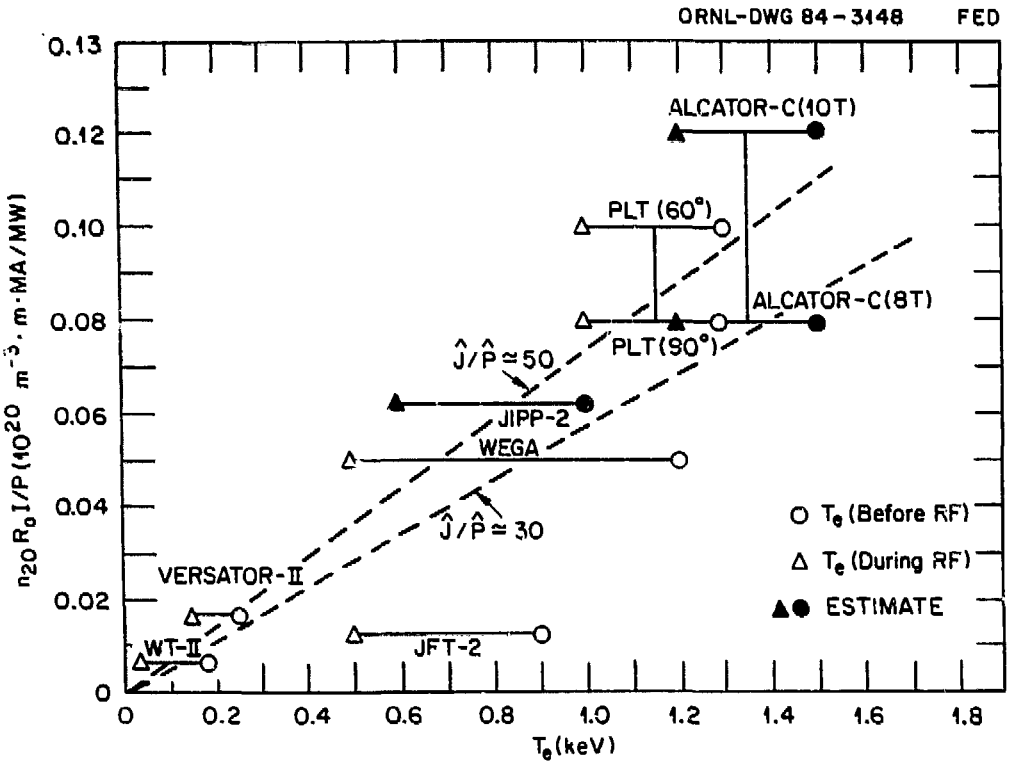

Fig. 12. Current drive efficiency vs T_e for a number of LHCD tokamak experiments (courtesy of N. Uckan, ORNL).

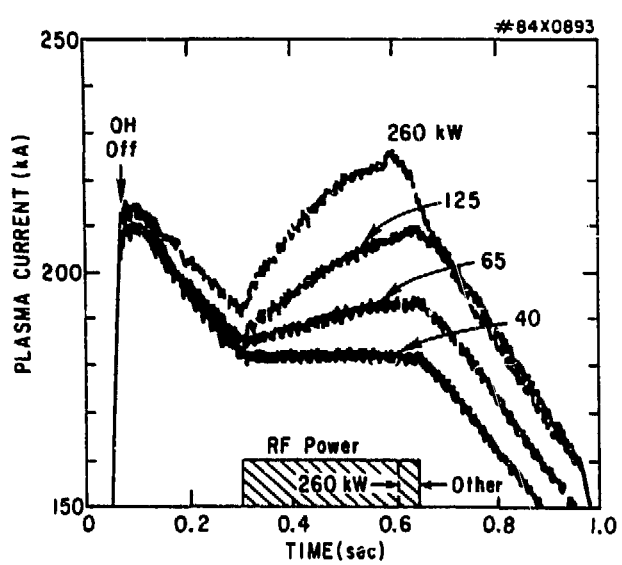

Fig. 13. Efficient current rampup is obtained in PLT using LHCD (courtesy of F. Jobes, PPPL).

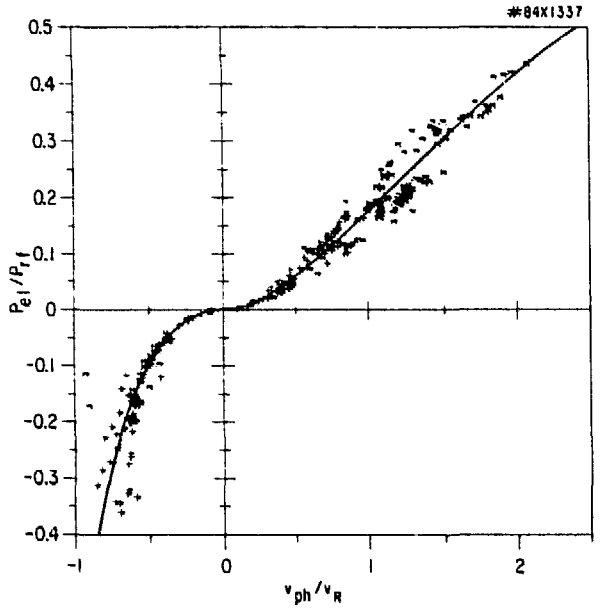

Fig. 14. P_{el}/P_{rf} vs V_{ph}/v_R where P_{el} is the power from the electrons going into the poloidal field energy and v_R is the runaway velocity for 250 PLT shots. The rf power varied from 0 to 300 kW; the density, from 1.5×10^{18} cm $^{-3}$ to 6.0×10^{18} m^{-3}; and the plasma current, from 150 to 400 kA. Three waveguide phasings were used: 60°(*), 90°(+), and 135°(#) (courtesy of N. Fisch, PPPL).

II. HEATING TO IGNITION

II.1 Heating Requirements

A detailed solution of Eqs. (I.1–I.14), showing the evolution of the radial profiles of the various quantities and allowing for a noncircular plasma, may be obtained using 1½-D codes such as the WHIST code.[6] For the purpose of providing a simpler solution, an average answer may be obtained by integrating the equations over the minor radius using model profiles for density and temperature.[47] As a further simplification, Eqs. (I.3) and (I.4) are combined to give

$$\frac{\partial}{\partial t}\left[\frac{3}{2}n_e(T_e + T_i)\right] = \frac{1}{r}\frac{\partial}{\partial r}\, r\left[ne\left(\chi_e \frac{T_e}{\partial r} + \chi_i \frac{\partial T_i}{\partial r}\right)\right] - p_b + p_\Omega + p_\alpha + p_a \qquad \text{(II.1)}$$

where the diffusion terms have been neglected in comparison with the conduction terms. The cyclotron radiation term is smaller than the bremsstrahlung term for most startup conditions in a D-T plasma and has been dropped. The line radiation and charge exchange terms are important at the edge of the plasma, but for a clean dense plasma they play only a small role in the central region and have been dropped.

Equation (II.1) is now multiplied by $4\pi^2 rR$ and is integrated over the minor radius, assuming that $n = n_0$ and $T = T_0(1 - r^2/a^2)$.

Ignoring the plasma edge region, and taking the temperature gradients at r/a = 0.8, Eq. (II.1) becomes

$$\frac{\partial}{\partial t} W \approx -0.16Rn_{19}(\chi_e T_{ek} + \chi_i T_{ik})$$

$$- 1.1 \times 10^{-3} RabT_{ek}^{0.5} Z_{eff}\, n_{19}^2 + \frac{0.12 Z_{eff} R I_M^2}{abT_{ek}^{1.5}}$$

$$+ 1.9 \times 10^{-4} Rabn_{19}^2 T_{ik}^{2.5} + P_\alpha \text{ (MW)} , \qquad \text{(II.2)}$$

where the total plasma energy is denoted by $W = (9.5 \times 10^{-2})Rabn_{19}(T_{ek} + T_{ik})$ (MJ); average values have been used for $\xi = 1.1$; $\gamma_R = 1.5$, and $\ln \Lambda = 19$; and I_M is the plasma current in MA. The alpha power formula ($P_\alpha \propto T_{ik}^{2.5}$) is a best fit for a parabolic temperature distribution for $2 \lesssim T_{ik} \lesssim 10$ keV, and n_{19} (10^{19} m^{-3}) and T_{ik} (keV) are average values. The results have been generalized to include a noncircular cross section.

II.2 Auxiliary Heating

Example 1: $n_{19} = 2.5$, $T_{ek} = T_{ik} = 2$, $\chi_e = 1.5$ m$^2 \cdot$s^{-1}, $\chi_i = 0.2$ m$^2 \cdot$s^{-1}, $R = 2$ m, $a = 0.8$ m, $b = 1.4$ m, $Z_{eff} = 1.5$, $I_M = 6$, $P_a = 0$,

$$\frac{\partial}{\partial t} W = -1.4 - 0.03 + 4.1 + 0.02 \text{ MW} ,$$

where the terms on the right side are conduction losses, bremsstrahlung losses, ohmic heating, and alpha power; and the ohmic temperature will rise to about 3 keV.

Example 2: $n_{19} = 25.0$, $T_{ek} = T_{ik} = 10$, $\chi_e = 0.2$ m$^2 \cdot$s^{-1}, $\chi_i = 0.7$ m$^2 \cdot$s^{-1}, $R = 2$ m, $a = 0.8$ m, $b = 1.4$ m, $Z_{eff} = 1.5$, $I_M = 10$, $P_a = 0$,

$$\frac{\partial}{\partial t} W = -7.2 - 7.3 + 1.0 + 84 \text{ MW} ,$$

again, where the terms on the right side are conduction losses, bremsstrahlung losses, ohmic heating, and alpha power; and in this case the plasma is ignited. Note that bremsstrahlung losses are about 10% of conduction losses, a typical value. Auxiliary power is required to bridge the gap between the ohmic temperature (~3 keV) and the ignition temperature (~10 keV) as illustrated in Fig. 15 in the form suggested by Wort.[48]

Setting $T_{ek} = T_{ik} = T_k$, $W = 0.19\text{RabE}n_{19}T_k$, and $\chi_e + \chi_i = \chi_E'(T_k/10)^\delta$, Eq. (II.2) may be rewritten as

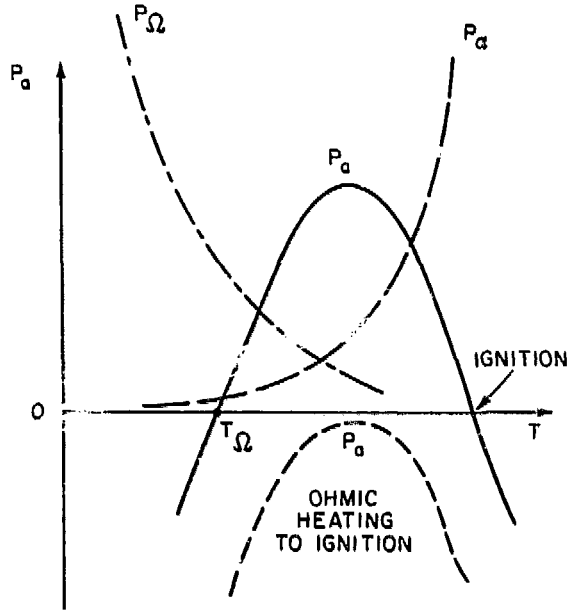

Fig. 15. Auxiliary power requirements for tokamaks have a characteristic variation with plasma temperature owing to the temperature dependences of ohmic, bremsstrahlung and alpha power.[48]

$$\frac{\partial}{\partial t}(C_0 T_k) = -C_1 T_{ik}^{1+\delta} - C_2 T_k^{0.5} + C_3 T_k^{1.5} + C_4 T_k^{2.5} + P_\alpha \ , \qquad \text{(II.3)}$$

where for neoclassical losses $\delta = -0.5$ (ref. 49), for neo-Alcator scaling $\delta = 0$ (ref. 50), and for auxiliary heating electron losses $\delta \simeq 0$ to -0.5 (refs. 51, 52) at constant beta or power, so that practically, in present tokamaks, the dependence of χ_E on temperature is observed to be weak.

The maximum auxiliary power occurs at $\partial W/\partial t = 0$ and comes mainly from balancing alpha power against conduction losses.

$$P_{am} = C_1 T_{mk}^{1+\delta} + C_2 T_{mk}^{0.5} - C_3 T_{mk}^{-1.5} - C_4 T_{mk}^{2.5} \ , \qquad \text{(II.4)}$$

where

$$T_{mk} = \left[\frac{350(1+\delta)\chi_E'}{abn_{19}}\right]^{1/(1.5-\delta)} .$$

Example 3: $n_{19} = 22$, $\delta = 0$, $\chi_E' = 1.0\ \mathrm{m^2 \cdot s^{-1}}$, $R = 2$ m, $a = 0.8$ m, $b = 1.4$ m, $Z_{eff} = 1.5$, $I_M = 10$ MA

$$P_{am} = 42 + 4 - 2 - 17 = 27\ \mathrm{MW} \ ,$$

where the four terms are conduction losses, bremsstrahlung losses, ohmic heating, and alpha power.

To raise the temperature to ignition in a finite time more auxiliary power is required to handle the thermal capacity of the plasma W. If one assumes a characteristic rise time of 5 s at $T_k = 5.9$ keV, then the term $\partial W/\partial t = 11$ MW, giving a total auxiliary heating requirement of $P_a = 38$ MW.

II.3 Ohmic Heating

At very high magnetic fields ($B_t > 10$ T) and at low q_ψ in small devices, it is possible to ignite ohmically.[8] Consider the case of neo-Alcator electron confinement,[50] shown in Eq. (II.12) with ion losses ignored.

The requirement for ohmic ignition is that $P_{am} < 0$. The position of the T_k maximum occurs approximately when $P_\alpha = P_\Omega$, since P_α is increasing with T_k while P_Ω is decreasing:

$$T_{m\Omega}\,(\text{keV}) \simeq 5.0 Z_{\text{eff}}^{0.5} \left(\frac{I_M}{abn_{19}} \right)^{0.5} , \tag{II.5}$$

and the ignition requirement is

$$\frac{0.24\, Z_{\text{eff}} R I_M^2}{abT_{m\Omega}^{1.5}} > \frac{6.9 b T_{m\Omega}}{q_{\text{cyl}} R} + 1.1 \times 10^{-3}\, Rab\, T_{m\Omega}^{0.5}\, Z_{\text{eff}}\, n_{19}^2$$

where q_{cyl} is defined in Eq. (II.7).

Example 4: $n_{19} = 80$, $I_M = 10$ MA, $q_{\text{cyl}} = 1.7$, $R = 1.0$ m, $a = 0.4$ m, $b = 0.7$ m, $Z_{\text{eff}} = 1.0$.

$$T_{m\Omega} = 3.34 \text{ keV} ,$$

and ohmic ignition occurs because the combined ohmic heating and alpha power is greater than the conduction and bremsstrahlung losses,

$$14.0 > 9.5 + 3.6 .$$

This simple model indicates the possibility of ohmic ignition. However , more careful modeling is required to account for the effects of sawtooth oscillations which enhance losses in the central region and modify the profiles; impurity radiation; ion losses, since at high density and low temperature $\chi_i \sim \chi_e$; and for trapped particle effects. A POPCON plot for ohmic ignition is given in Fig. 2b.

A good representation of the relationship between plasma current, toroidal field and MHD safety factor (q_ψ) is given by

$$I_M = \frac{2.5\, a^2 B_t (1.22 - 0.68 a/R)(1 + b^2/a^2)}{q_\psi R (1 - a^2/R^2)^2} \quad (\text{MA}) . \tag{II.6}$$

The q_{cyl} is defined as

$$q_{cyl} = \frac{2.5\, a^2 B_t}{R\, I_M} \left[1 + \frac{b^2}{a^2}\right] . \tag{II.7}$$

Thus for the example above the requirement is $B_t = 12.1$ T.

II.4 Ignition Constraints

In tokamak operation a number of practical constraints are found to apply, some of which may be explained theoretically. With careful control or the use of a close-fitting conducting shell, tokamaks have been operated to low values of q_ψ [~1.3 (ref. 53)]. In practice, this is not commonly achieved because of the difficulty of crossing the $q_\psi = 2$ boundary stably. At these low q_ψ values the $q = 1$ surface is observed to be at relatively large minor radius, and most of the confinement is supported by steep gradients near the edge. If it were possible to stabilize the $m = 1$ mode, then the low-q_ψ mode of operation would permit relatively large I_p, ignited operation at low poloidal beta β_{pol}, and easier ohmic access to ignition. The commonly accepted standard, however, is $q_\psi \gtrsim 2.5$.

The density is limited by the Murakami limit[5] to

$$n_m \leqslant \nu_m \frac{B_t}{R q_{cyl}} , \tag{II.8}$$

where

$\nu_m \simeq 1.5$ for ohmically heated plasmas,

$\nu_m \simeq 2.0$–$3.0$for auxiliary heated plasmas.

The cause of the limit is not clearly established, though it may relate to whether there is adequate power to sustain a stable edge region. Certainly, above the limit in ohmic plasmas the current channel has been observed to shrink, leading to disruption. The operating space is illustrated in the Hugill diagram[54] shown in Fig. 16.

Theoretical limits have been established for the volume average beta using MHD codes; and experimental data from ISX-B, DIII, Asdex, JFT-2, and TOSCA T-11 are in rough agreement with the predictions. The limits may be set by external kink modes or by ballooning modes. The so-called Troyon limit on beta[4] is

$$\langle \beta \rangle_m \simeq (0.03 - 0.04) \frac{I_M}{a B_t} . \tag{II.9}$$

These limits are used in the POPCON plots shown in Fig. 2.

There exist a plethora of confinement scalings. For the ions' neoclassical losses including finite aspect, ratio corrections are given by the Chang-Hinton formula.[49]

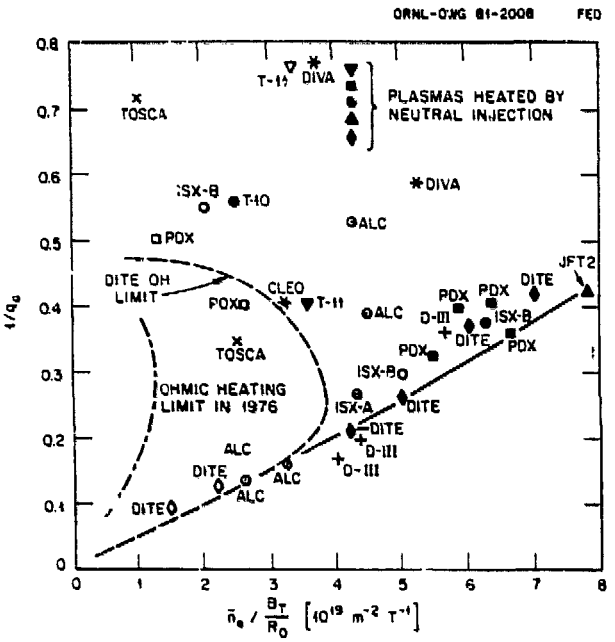

Fig. 16. The extension of the operational space in a tokamak is illustrated by the expanded ohmic heating region obtained with improved plasma purity and by the greater range obtained with auxiliary heating (the solid points).

$$\chi_{iCH} = \frac{1.3 \times 10^{-2} K^* n_{19} Z_{eff} T_{ik}^{0.5} \epsilon^{-1.5} q_{cyl}^2 B_t^{-2}}{(1 + b^2/a^2)} , \qquad \text{(II.12)}$$

where

$$K^* = (0.66 + 1.88\epsilon^{0.5} - 1.54\epsilon)(1 + 1.5\epsilon^2) , \quad \epsilon = \frac{r}{R} .$$

For the electrons with ohmic heating the simplest formula that fits both small and large tokamaks is the "neo-Alcator scaling":[50]

$$\chi_{e,NA} = \frac{43\, b}{n_{19} R^2 q_{cyl}} \quad (m^2 \cdot s^{-1}) . \qquad \text{(II.13)}$$

For the auxiliary heating case it is observed that generally χ_e may rise above $\chi_{e,NA}$ by a factor of 4. Data from Asdex[56] and ISX-B[57] show that improved confinement can be obtained when the edge temperature gradient is steep enough. For the poor confinement (L-mode) case, Kaye and Goldston[51] have made an empirical fit to χ_e :

$$\chi_{e,KG} = \frac{5.9 \langle n_{19} \rangle^{0.76} \langle T_{ek} \rangle^{1.38} a^{3.38} B_t^{0.21} \kappa^{1.71}}{I_M^{2.95} A_j^{2.55}} \left(\frac{2\kappa^2}{1 + \kappa^2} \right) (m^2 \cdot s^{-1}) , \qquad \text{(II.14)}$$

$$\kappa = \frac{b}{a} .$$

With auxiliary heating confinement improves with increasing plasma current, and a form of the Gorbunov-Mirnov-Strelkov scaling[52] is a fair fit to data:

$$\chi_{e,L} = \frac{2a}{I_M \kappa^{1/2}} \left(\frac{2\kappa^2}{1 + \kappa^2} \right) \ (m^2 \cdot s^{-1}) \ . \tag{II.15}$$

For the high confinement or H-mode cases,

$$\chi_{e,H} = \frac{(0.75 - 1.0)a}{I_M \kappa^{1/2}} \left(\frac{2\kappa^2}{1 + \kappa^2} \right) \ (m^2 \cdot s^{-1}) \ . \tag{II.16}$$

As a rule of thumb, $\chi_{e,H} \gtrsim 1.4\ \chi_{e,NA}$ with auxiliary heating.

II.5 Confinement Scalings

The ignition condition ($M = 1$) and the ignition margin (M) subject to the above constraints may be written as[55]

$$M\left[\chi_e \frac{T_{ek}}{T_{ik}} + \chi_i\right] \simeq 0.22 f_\alpha \langle\beta\rangle B_t^2 \ ab \ , \tag{II.10}$$

where $f_\alpha \simeq 0.8$ represents the portion of alpha power available to support radial conduction losses. Combining Eqs. (II.8) and (II.9) leads to

$$M\left[\chi_e \frac{T_{ek}}{T_{ik}} + \chi_i\right] \simeq (6.6 - 8.8) \times 10^{-3} f_\alpha I_M B_t \ b \ , \tag{II.11}$$

which gives the maximum margin subject to the beta limit. For example, if $T_{ek} = T_{ik}$, $\chi_e = \chi_i = 0.2\ m^2 \cdot s^{-1}$, $f_\alpha = 0.8$, $I_M = 10$ MA, $B_t = 8$ T, and $b = 1$ m, then $M = 1.1$–1.4.

II.6. Auxiliary Heating Methods

The most successful approaches to the auxiliary (nonohmic) heating of tokamaks have been the injection of intense neutral atom beams,[58] the application of rf heating,[59] and adiabatic compression.[60] In addition, plasma fueling has advanced with the use of solid hydrogen pellet injection alone.[61] Figure 17 illustrates the increase in operating range achieved with these techniques. Figure 18 illustrates the heating techniques.

II.6.1. Neutral beam injection

This heating technique involves injecting an intense beam of energetic atoms, generally hydrogen or deuterium, into the plasma. Typical injection energies lie in the range from 10 to 100 keV for present experiments. Systems have been developed up to 150 keV. Because the atoms are neutral, they can cross the outer regions of the confining magnetic field and reach the plasma. The atoms penetrate

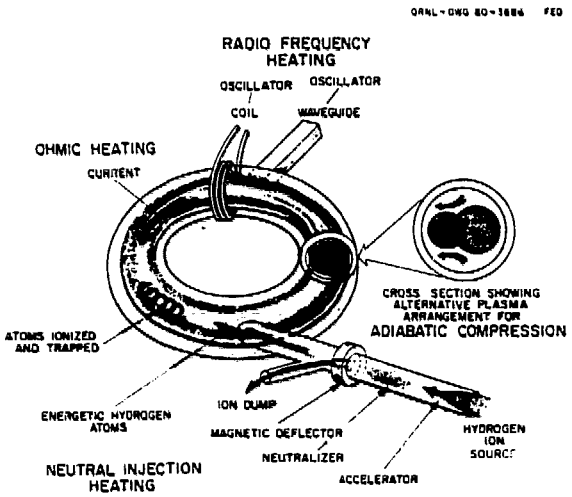

Fig. 17. An illustration of the main heating systems that have been used on tokamaks.

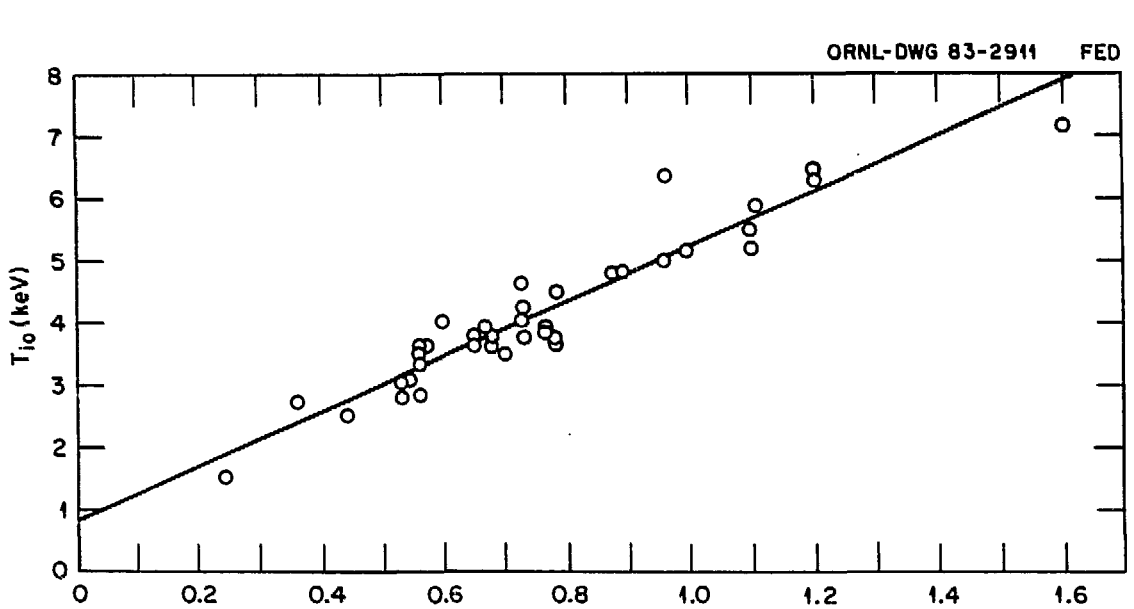

Fig. 18. The central ion temperature on PLT increases linearly with neutral injection power normalized to the density (courtesy of H. Eubank, PPPL).

the plasma until they are either ionized or charge exchange on plasma ions. In most applications a small percentage of the beam passes through the plasma. The energetic ions produced are then trapped by the magnetic field and orbit within the plasma, slowing down by collisions that heat the plasma. Some of the ions may be trapped on orbits that intersect the limiter and walls. Other energetic ions may suffer collisions that transfer them into uncontained orbits as they slow down. In practice, for most applications conditions are set up in which the total loss of power is <20%.

Neutral beams may be used to heat the ions directly. The fraction of power transferred to the ions depends upon the critical energy E_c (ref. 17). In general, for an ion of atomic number A and mass M, slowing down on a plasma A_j, M_j, the critical energy at which the power transfer rate to plasma ions and electrons is equal[17] is

$$E_c = 14.8 T_{ek} \left[\frac{A^{3/2}}{n_e} \sum \left[\frac{n_j Z_j^2}{A_j} \right] \right]^{2/3} . \tag{II.17}$$

The first demonstration of substantial ion heating in the reactor plasma region was on PLT (ref. 62), where plasma temperatures were raised to $T_i(0) \rightarrow 7.5$ keV, $T_e(0) \rightarrow 3.5$ keV. The increase of ion temperature with power is illustrated in Fig. 18. Because the beam ions have a finite slowing-down time, they also contribute to the mean ion energy and to beta. In PLT the mean central ion temperature was raised to 13 keV. Similar parameters have now been achieved in PDX and DIII. For deuterium beam injection into a D-T plasma, the energetic ions can fuse, thereby enhancing the alpha power in the plasma.[63]

II.6.2 RF Heating

This technique involves driving oscillatory currents in the plasma at frequencies for which the plasma impedance is high. In fusion, the term rf heating is used loosely for systems operating at frequencies in the range from 30 kHz to 250 GHz. Each system consists of a high-power oscillator with feed cables or waveguides going to a launching structure made of coils or waveguides that are close to the plasma (see Fig. 17). There are a number of stages involved.

Generation: This is the efficient production of power at the given frequency. Sources are available with $\gtrsim 50\%$ efficiency operating continuous wave (cw) with unit size in the range from 100 kW to 1 MW at frequencies up to ~ 10 GHz. For higher frequencies the gyrotron is being developed, and a tube operating cw at 200 kW, 60 GHz, with $\sim 40\%$ efficiency has been tested.[64] Good progress is being made in the development of 140 GHz gyrotrons.[65]

Transmission coupling: This is the efficient coupling of power, which requires that the power penetrate and be absorbed by the plasma. If the phase velocity of the wave $\omega/k \rightarrow \infty$, the wave is reflected. This is called "cutoff." In the absence of a magnetic field, cutoff occurs at an incident frequency $\omega = \omega_{pe}$ (the electron plasma frequency). In the presence of a magnetic field, electron motion is constrained; depending on the polarization of the wave, penetration may occur at a slightly lower frequency. Propagation occurs provided the density remains below a value corresponding to cutoff,

$$n_{max} = 1.24 \times 10^{18} \, (\mathrm{m}^{-3}) \left(\frac{\omega}{10 \text{ GHz}} \right)^2 \times \begin{cases} 1 + \dfrac{1}{m} \text{ , extraordinary mode } (E_\omega \perp B) \\ 1 \text{ , ordinary mode } (E_\omega \parallel B) \end{cases} \tag{II.18}$$

where ω and $k = 2\pi/\lambda$ are the incident wave frequency and wave numbers, respectively, and m is the cyclotron harmonic number.

In practice, rf heating is used at frequencies well below cutoff; lower hybrid heating (LHH) and ICH are examples. In this situation the finite geometry of the plasma and launching system is important (i.e., $\lambda \sim a$). The near field of the launching structure is used to excite oscillations in the plasma, and under suitable circumstances these in turn drive waves. This effect is called mode conversion, and it leads to the propagation of power into the interior of the plasma.

Absorption: For good absorption it is necessary for the phase velocity of the propagating wave to match the velocity v_q of either the electrons ($q = e$) or the ions ($q = i$). More generally the requirement is $(\omega - m\omega_{cq})/k \to v_q$ where m is an integer ion and ω_{cq} is the cyclotron frequency. The thermalization of power by the particles resonant with the wave may be by collisions, Landau damping or cyclotron damping or at very high power densities by nonlinear interactions resulting from turbulence generated by the incident wave.

The attractions of rf heating are that, in principle, the power may be preferentially deposited in the resonant region, which may be selected; either electrons or ions may be heated; and as discussed in Sect. I.4.4, momentum may be transferred to the plasma in a way that drives a parallel current. Because the components near the plasma may be simpler than those of neutral injection, rf heating has become the preferred technique for ignition experiments that require remote handling.[1-3] Some characteristics of major heating regimes and experimental results are given in Table II.1.

Ion cyclotron heating: This technique has been applied to a large number of experiments, for example, on PLT[66] and TFR[67], and with notable success on PLT, where the ion temperature has been raised to 5 keV. The increase of ion temperature with increasing rf power is shown in Fig. 19. A main issue for ICH is the

Table II.1. Characteristics of major rf heating regimes and experimental results

Regime	Ion cyclotron range		Lower hybrid range		Electron cyclotron range	
Frequency GHz	10^{-3}, 10^{-2}, 10^{-1}		10^{-0}–10^{-1}		10^{2}	
Dominant Heating	Ion		Ion/electron		Electron	
	Device					
	TFR	PLT	Alcator-C	PLT	DIII	T-10
Results						
n_{e0} ($\times 10^{19}$m^{-3})	11	5.5	25	1.5	3	5
T_{e0} (keV)	1.3	5.0	2.0	1.5	–	–
T_{i0} (keV)	–	4.0	3.4	4.5	4.0	2.5
Power (MW)	0.7	5.3	0.85	0.5	0.53	1.0

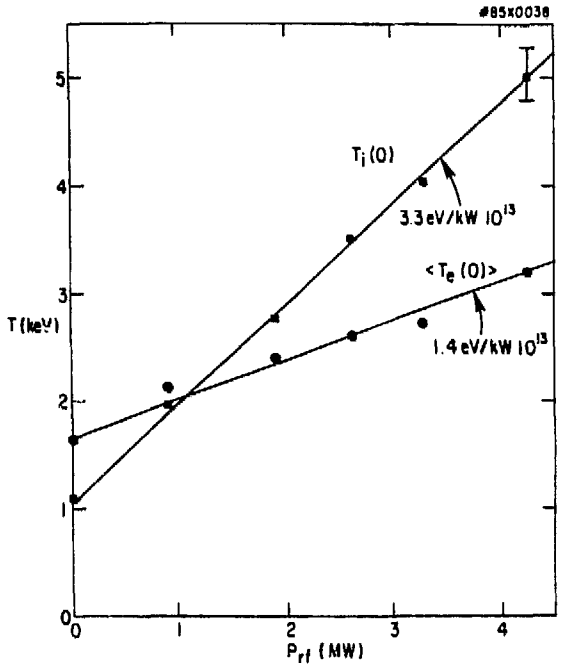

Fig. 19. High temperatures for both ions and electrons are obtained by ICH in PLT (courtesy of J. Hosea, PPPL).

observed problem of impurity generation by the technique. It is hoped that this will be overcome by better launching structure design.

There are a variety of resonances to which power may be coupled: (1) the harmonics of the ion cyclotron frequency, and (2) when two ion species are present, the hybrid frequency. Most of the work has been directed at heating a minority H or ^{3}He component in a deuterium plasma. The region of power deposition depends upon the fraction $\eta = n_H/n_D$ or $n_{^3He}/n_D$. For $\eta \sim 0.05$ the power is absorbed at the minority cyclotron frequency, providing a very energetic minority component; this component then slows down in a manner similar to the energetic ions in neutral injection, heating both electrons and ions. For larger η ($\gtrsim 0.1$), the wave is dampened near the ion hybrid resonant layer by electron Landau damping and at the minority resonance by cyclotron damping, again leading to both electron and ion heating. Power has also been coupled successfully at the second harmonic frequency of hydrogen.

Lower hybrid heating: Waveguides may be used for launching, even in modest-size, present-day tokamaks. Access to the resonance zone requires the incident wave to have a finite wave number parallel to the magnetic field. This may be provided by using a set of waveguides with the wave phase alternated—the Brambilla grill.[68] Experiments at low power show that the coupling varies as a function of phase angle, in agreement with the Brambilla theory. At high power nonlinear effects occur,[69] and the problem of power absorption near the launching structure is a key research topic. Substantial heating has been demonstrated in Alcator C (ref. 70) and PLT (ref. 23) as shown in Fig. 20.

Electron cyclotron heating: In this technique power is coupled to harmonics of the electron cyclotron frequency, generally to the first or second harmonic. Because

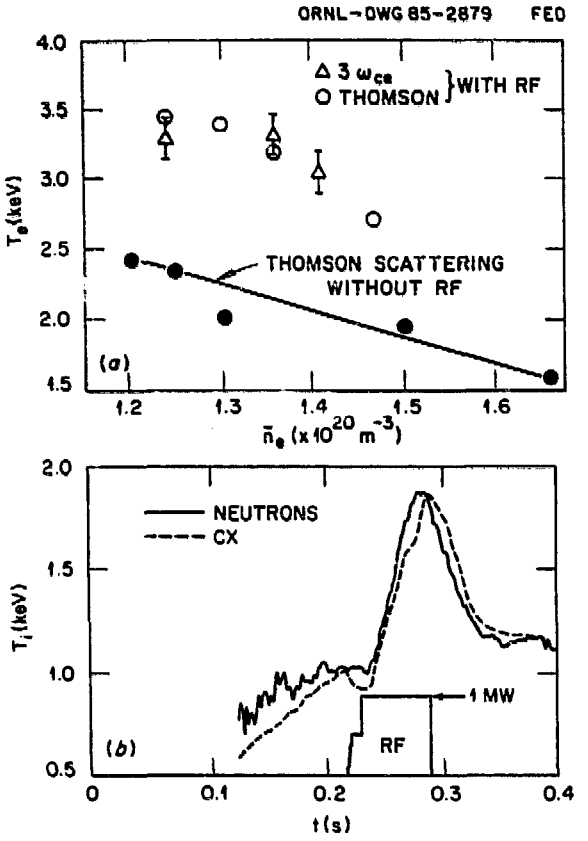

Fig. 20. A substantial electron temperature rise is obtained in Alcator-C by lower hybrid heating (courtesy of M. Porkolab, MIT).

these are high frequencies in the plasma devices and $\lambda << a$, it is necessary in principle to satisfy the cutoff condition [Eq. (II.17)], although an unexplained coupling has been observed above the cutoff in DIII. The main problem in the 1970s was the lack of efficient high-power sources. This problem has been overcome by the development of the gyrotron, and numerous successful applications of ECH have been made. A substantial program in T-10 (ref. 71) has demonstrated both heating and the ability to modify MHD activity. The optimization of up to 1 MW of power at 60 GHz in DIII (ref. 72) has led to substantial electron heating, as illustrated in Fig. 2.

II.6.3 Adiabatic compression

Major-radius adiabatic compression was first demonstrated on ATC (ref. 60) and has been explored further in TFTR (ref. 73). It is viewed generally as a backup possibility, since it imposes constraints on the coil system and structure owing to the fast rates of field rise required. It has been considered for specialized ignition devices such as Zephyr (ref. 74).

III CONCLUSIONS

Substantial progress has been made in recent years in all aspects of tokamak startup. It now appears possible to preionize the plasma to raise the plasma current to the maximum level using rf heating and noninductive current drive. These techniques permit substantial simplification of the poloidal coil system, vacuum vessel,

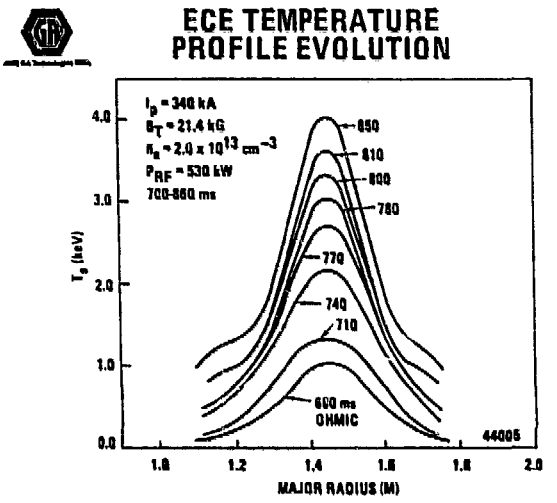

Fig. 21. High electron temperatures are obtained in DIII with ECH heating (courtesy of R. Prater, GAT).

and structure. In addition, there are a variety of techniques for bulk heating the plasma to ignition efficiently.

ACKNOWLEDGMENTS

I appreciate the help of S. Borowski, W. A. Houlberg, N. A. Uckan (ORNL); R. Prater (GAT); M. Porkolab, and S. Wolfe (MIT); and S. Bernabei, P. Colestock, J. Hosea, and F. Jobes (PPPL). The INTOR and FED/TFCX studies were very useful in providing background information and a format for this paper.

LIST OF SYMBOLS (UNITS)

a (m)	small minor radius
A	atomic number
a_{pol} (m)	poloidal coil radius
b (m)	large minor radius
B_t (T)	toroidal magnetic field
$B_\perp$ (T)	poloidal stray magnetic fields
D_A ($m^2 \cdot s^{-1}$)	ambipolar diffusion rate
D_e ($m^2 \cdot s^{-1}$)	electron diffusion rate
D_i ($m^2 \cdot s^{-1}$)	ion diffusion rate
E_n (eV)	energy of fusion neutron
f_α	portion of alpha power available to support radial conduction losses
I_M (MA)	plasma current in megamperes
I_p (A)	plasma current
I_{rf} (MA)	rf current
j ($A \cdot m^{-2}$)	plasma current density
$\hat{J}$	normalized J, J/nev_e
k (m^{-1})	wave number, $2\pi/\gamma$
L (H)	plasma inductance
m_e (kg)	electron mass
m_i (kg)	ion mass
M	ignition condition
n (m^{-3})	density
n_D (m^{-3})	deuterium density
n_e (m^{-3})	electron density
$\bar{n}_e$ (m^{-3})	average electron density
n_i (m^{-3})	ion density
n_m (m^{-3})	maximum density
n_n (m^{-3})	neutral density
n_T (m^{-3})	tritium density
n_0 (m^{-3})	oxygen density
n_{19}	density (10^{19} m^{-3})
p (torr)	pressure
p_a ($W \cdot m^3$)	auxiliary power density
p_b ($W \cdot m^3$)	bremsstrahlung power density
p_c ($W \cdot m^3$)	cyclotron radiation power density
p_{cx} ($W \cdot m^3$)	charge-exchange power density
p_{ei} ($W \cdot m^3$)	electron-ion heat transfer
p_F ($W \cdot m^3$)	fusion power density
p_{ie} ($W \cdot m^3$)	ion-electron heat transfer
p_R ($W \cdot m^3$)	radiation power density
p_α ($W \cdot m^3$)	alpha power density
p_μ ($W \cdot m^3$)	microwave power density
p_Ω ($W \cdot m^3$)	ohmic heating power density
P (W)	power
$\hat{P}$	normalized power, $P/m_e n v_e^2 \nu_0$
P_a (MW)	auxiliary power
P_{am} (MW)	maximum auxiliary power
P_{rf} (MW)	rf heating power
P_μ (MW)	microwave power

q	safety factor
q_ψ	MHD safety factor
q_0	safety factor at the center of the plasma
Q	energy gain
r (m)	radius
R (m)	major radius
R_e	wall reflectivitiy
R_p (ohm)	plasma resistance
t (s)	time
T (eV)	temperature
T_e (eV)	electron temperature
$\overline{T_e}$ (eV)	average electron temperature
T_{ek} (keV)	T_e in kilo electron volts
T_{e0} (eV)	central electron temperature
T_i (eV)	ion temperature
T_{ik} (keV)	T_i in kilo electron volts
T_{i0} (eV)	central ion temperature
T_k (keV)	temperature in kilo electron volts
T_Z (eV)	impurity temperature
U (V)	loop voltage
U_0	V_{rel}/v_e
v_e ($m \cdot s^{-1}$)	electron thermal speed
V_{ph} ($m \cdot s^{-1}$)	phase velocity
V_{rel} ($m \cdot s^{-1}$)	relative velocity of ion and electron species
W (MJ)	thermal capacity of the plasma
Z	charge state of impurity ion
Z_{eff}	effective Z, $\sum (Z^2 n_Z + n_i)/n_e$
β_{pol}	poloidal beta
γ_R	correction factor allowing for trapped electron effects
ϵ	r/R
ϵ_i (eV)	effective ionization energy for hydrogen
$\eta_\parallel$ (ohm·m)	parallel resistivity
κ	b/a
μ_0 ($H \cdot m^{-1}$)	magnetic moment
ν (s^{-1})	collision frequency
ν_{ei} (s^{-1})	electron-ion collision frequency
ξ	correction for e-e collisons and relativistic effects
$\langle \sigma v \rangle_{cx}$ ($cm^3 \cdot s^{-1}$)	charge-exchange rate coefficient
$\langle \sigma v \rangle_F$ ($cm^3 \cdot s^{-1}$)	fusion rate coefficient
$\langle \sigma v \rangle_i$ ($cm^3 \cdot s^{-1}$)	ionization rate coefficient
τ (s)	confinement time
χ_e ($m^2 s^{-1}$)	electron thermal diffusivity
χ_i ($m^2 s^{-1}$)	ion thermal diffusivity
ω ($rad \cdot s^{-1}$)	incident wave frequency
ω_{ce} ($rad \cdot s^{-1}$)	electron cylotron frequency
ω_{LH} ($rad \cdot s^{-1}$)	lower hybrid frequency
ω_{pe} ($rad \cdot s^{-1}$)	electron plasma frequency
ω_{pi} ($rad \cdot s^{-1}$)	ion piasma frequency
Ω_e ($rad \cdot s^{-1}$)	electron cyclotron frequency
$\langle ... \rangle$	average

REFERENCES

1. Shannon, T. E., et al., *International Tokamak Reactor, Phase One and Phase Two*, (report of the INTOR Workshop held in seven sessions, Vienna, 1981–1983), IAEA, Vienna, 1983.
2. Flanagan, C. A., et al., *Fusion Engineering Device Design Description*, Oak Ridge National Laboratory Report ORNL/TM-7948, 1981.
3. *TFCX Preconceptual Design Report: Overview*, Princeton Plasma Physics Laboratory Report PPPL, F-A-8407-006, 1984.
4. Troyon, F., et al., *Plasma Phys.* **25**, 209 (1984).
5. Murakami, M., et al., *Nucl. Fusion* **16**, 347 (1976).
6. Houlberg, W. A., et al., *Nucl. Fusion* **22**, 935 (1982).
7. Watkins, M. L., et al., *Proceedings of the 8th International Conference on Plasma Physics and Controlled Nuclear Fusion Research (Brussels, 1980)*, IAEA, Vienna, vol. 1, p. 639, 1981.
8. Coppi, B., *Comments Plasma Phys.* **3**, 2 (1977).
9. Freeman, R. L., and Jones, E. M., *Atomic Collision Processes in Plasma Physics Experiments*, Culham Laboratory Report CLM-R-137, Abingdon, England, 1974.
10. Burrell, K. H., et al., *Phys. Rev. Lett.* **41**, 1382 (1978).
11. Stacey, W. M., Jr., and Sigmar, D. J., *Nucl. Fusion* **19**, 1665 (1979).
12. Dei-Cas, R., et al., *J. Nucl. Mater.* **76**, 542 (1978).
13. Braginskii, S. I., in *Reviews of Plasma Physics*, edited by M. A. Leontovich (Consultants Bureau, New York, 1965), vol. 1, p. 205.
14. Rose, D. J., and Clarke, M. C., *Plasma and Controlled Fusion* (John Wiley, Inc., New York, and MIT Press, Boston, 1961) p. 232.
15. Post, D. E., et al., *At. Data Nucl. Data Tables* **20**, 400 (1977).
16. Trubnikov, B., et al., p. 93 in *Second International Conference on Peaceful Uses of Atomic Energy (Geneva)*, vol. 31, 1958.
17. Stix, T. H., *Plasma Phys.* **14**, 367 (1972).
18. *U.S.S.R. Conceptual Design Contribution to the INTOR Phase 1 Workshop*, Kurchatov Institute, Moscow, 1981.
19. (a) Peng, Y-K. M., et al., *Nucl. Fusion* **18**, 1489 (1978). (b) Borowski, S. K. et al., *Fusion Technol.* **6**, 7 (1984).
20. Bulyginsky, D. G., et al., Ioffe Physical Institute Report No. 611, Leningrad, U.S.S.R., 1979.
21. Gilgenbach, R. M., et al., *Nucl. Fusion* **21**, 319 (1981).
22. Alikaev, V. V., et al., *Sov. J. Plasma Phys* **9**, 196 (1983).
23. Jobes, F. C., et al., presented at the RF Plasma Heating Conference, Callaway, Georgia, 1985 (to be published in AIP Conference Proceedings).
24. Sager, P. H., et al., *FED Baseline Engineering Studies Report*, Oak Ridge National Laboratory Report ORNL/FEDC-82/2, 1983.
25. Wesson, J. A., *Nucl. Fusion* **18**, 87 (1978).
26. Sheffield, J., and Gibson, A., *Nucl. Fusion* **15**, 677 (1975).
27. Meyerhofer, D. D., et al., Princeton Plasma Physics Laboratory Report PPPL-2169, 1984.
28. Mirnov, S. V., and Semenov, I. B., *Sov. J. Plasma Phys.* **4**, 27 (1978).
29. Granetz, R. S., *Nucl. Fusion* **19**, 1587 (1979).
30. Furth, H. P., et al., *Phys. Fluids* **16**, 1054 (1973).
31. Karger, K., et al., post-deadline paper A-10, in *Proceedings of the 11th European Conference on Controlled Fusion and Plasma Physics, Aachen, FRG*, September 1983.

32. Houlberg, W. A., and Hogan, J. T., *Nucl. Technol./Fusion* 3, 244 (1983).
33. Efthimion, P. C., et al., paper A-I-2 in *Proceedings of the 10th International Conference on Plasma Physics and Controlled Nuclear Fusion Research (London, 1984)*, IAEA, Vienna, 1985.
34. Rebut, P. C., et al., p. 10 in *Proceedings of the 10th International Conference on Plasma Physics and Controlled Nuclear Fusion Research (London, 1984)*, vol. 1, IAEA, Vienna, 1985.
35. Uckan, N. A., *Noninductive Current Drive in Tokamaks*, Oak Ridge National Laboratory Report ORNL/TM-9296.
36. Axon, K. B., et al., p. 413 in *Proceedings of the 8th International Conference on Plasma Physics and Controlled Nuclear Fusion Research (Brussels, 1980)*, vol. 1, IAEA, Vienna, 1980.
37. Helava, H., et al., *Bull. Am. Phys. Soc.* **25**, 952 (1980).
38. Fisch, N. J., *Phys. Rev. Lett.* **41**, 873 (1978); **42**, 410 (1979).
39. Cordey, J. G., *Plasma Phys.* **25**, 361 (1983).
40. Bernabei, S., et al., *Phys. Rev. Lett.* **49**, 1255 (1982).
41. Karney, C. F., and Fisch, N. J., *Phys. Fluids* **28**, 116 (1985).
42. Porkolab, M., et al., p. 529 in *Heating in Toroidal Plasmas: Proceedings of the 4th International Conference (Rome, 1984)*, vol. I, International School of Plasma Physics, Varenna, Italy, 1984.
43. Toi, K., et al., *Phys. Rev. Lett.* **52**, 2144 (1984).
44. Fisch, N. J., and Karney, C.F., *Phys. Rev. Lett.* **54**, 897 (1985).
45. Fisch, N. J., *Phys. Fluids* **28**, 245 (1985).
46. Jobes, F. C., et al., Princeton Plasma Physics Laboratory Report PPPL-2200, 1985.
47. Sheffield, J., "Tokamak Reactors for Breakeven," p. 511 in *Proceedings, Erice School on Tokamak Reactors for Breakeven*, Erice, Sicily, September 20–October 1, 1976.
48. Wort, D., p. 517 in *Proceedings B.N.E.S. Conference on Nuclear Fusion Reactor* (*Culham, England*), 1969.
49. Chang, C. S., and Hinton, F. L., *Phys. Fluids* **25**, 1493 (1982).
50. Blackwell, B., et al., p. 27. in *Proceedings of the 9th International Conference on Plasma Physics and Controlled Nuclear Fusion Research* (*Baltimore, 1982*), vol. II, IAEA, Vienna, 1983.
51. Kaye, S. M., and Goldston, R. J., *Nucl. Fusion* **25**, 65 (1985).
52. Gorbunov, E. T., et al., *Nucl. Fusion* **10**, 43 (1970).
53. DIVA Group, *Nucl. Fusion* **20**, 271 (1980).
54. Axon, K. B., et al., p. 51 in *Proceedings of the 7th International Conference on Plasma Physics and Controlled Fusion Research (Innsbruck, 1978)*, vol. I, IAEA, Vienna, 1979.
55. Sheffield, J., *Options for an Ignited Tokamak*, Oak Ridge National Laboratory Report ORNL/TM-8924, 1984.
56. Wagner, F., et al., p. 54 in *Proceedings of the 9th International Conference on Plasma Physics and Controlled Nuclear Fusion Research (Baltimore, 1982)*, vol. 1, IAEA, Vienna, 1983.
57. Wootton, A. J. et al., *J. Nucl. Mater.* **111 & 112**, 479 (1982).
58. Menon, M. M., *Proc. IEEE* **69**, 885 (1981).
59. Hwang, D. Q., and Wilson, J. R., *Proc. IEEE* **69**, 1030 (1981).
60. Bol, K., et al., p. 83 in *Proceedings of the 5th International Conference on Plasma Physics and Controlled Nuclear Fusion Research (Tokyo, 1974)*, vol. 1, IAEA, Vienna, 1975.
61. Milora, S. L., *J. Fusion Energy* **1**, 15 (1981).

62. Stodiek, W., et al., p. 9 in *Proceedings of the 8th International Conference on Plasma Physics and Controlled Nuclear Fusion Research (Brussels, 1980)*, vol. 1, IAEA, Vienna, 1980.
63. Jassby, D., et al., *Nucl. Fusion* **16**, 15 (1976).
64. Haste, G. R., private communication (Varian Associates), ORNL, 1985.
65. Haste, G. R., private communication (Varian Associates), ORNL, 1985.
66. Hosea, J. C., et al., presented at the RF Plasma Heating Conference, Callaway, Georgia, 1985 (to be published in AIP Conference Proceedings).
67. Adam, J., and Equipe TFR, p. 277 in *Heating in Toroidal Plasmas: Proceedings of the 4th International Symposium (Rome, 1984)*, vol. I, International School of Plasma Physics, Varenna, Italy, 1984.
68. Brambilla, M., *Nucl. Fusion* **16**, 47 (1976).
69. Dupas, L., et al., p. 489 in *Proceedings of the 8th International Conference on Plasma Physics and Controlled Nuclear Fusion Research (Brussels, 1980)*, vol. II, IAEA, Vienna, 1980.
70. Porkolab, M., et al., *Phys. Rev. Lett.* **53**, 1229 (1984).
71. Parail, V. V., and Alikaev, V. V., p. 753 in *Heating in Toroidal Plasmas: Proceedings of the 4th. International Symposium (Rome, 1984)*, vol. II, International School of Plasma Physics, Varenna, Italy, 1984.
72. Prater, R., et al., p. 763 in *Heating in Toroidal Plasmas: Proceedings of the 4th International Symposium (Rome, 1984)*, vol. II, International School of Plasma Physics, Varenna, Italy, 1984.
73. Tait, G., et al., Paper A-III-1 in *Proceedings of the 10th International Conference on Plasma Physics and Controlled Nuclear Fusion Research (London, 1984)*, IAEA, Vienna, 1985.
74. Andelfinger, C., et al., *Z. Naturforsch.* **37a**, 912 (1982).